JOURNAL OF CATALYSIS 88, 137–149 (1984)

A Fourier-Transform Infrared Spectral Study of H-ZSM-5 Surface Sites and Reactivity Sequences in Methanol Conversion

MOEIN B. SAYED, RONALD A. KYDD,[a] AND RALPH P. COONEY

Department of Chemistry, University of Newcastle, New South Wales, Australia, 2308

Received July 12, 1983; revised February 21, 1984

Surface sites on a series of dealuminated zeolitic catalysts of the H-ZSM-5 and mordenite types have been investigated using Fourier-transform–infrared spectroscopy (FT–ir). Three types of H-ZSM-5 surface site have been considered in detail: dealumination-associated Brønsted-silanol sites, aluminum-associated Brønsted-silanol sites, and Lewis sites. Sequences of populations of these sites have been identified using three methods: silanol stretching mode absorbance changes, relative changes in absorbance of adsorbed pyridine modes, and analytical data from X-ray fluorescence (XRF) characterizing the extracted surface layer. In the case of the method based on adsorbed pyridine a novel treatment has been developed which permits Brønsted (B)/Lewis(L) site ratios to be calculated as a function of temperature. This method reveals that the [B]/[L] ratio exhibits a maximum at ca. 473 K which is associated with the dealumination Brønsted sites. Comparison of sequences of site populations with observed reactivities suggests that Lewis sites are the origin of catalytic activity in the conversion of CH_3OH to $(CH_3)_2O$. Similar comparisons indicate that dealumination Brønsted sites are the principal source of reactivity for the conversion of $(CH_3)_2O$ to hydrocarbons. The migration of aluminum atoms away from the surfaces of ZSM-5 during calcination is invoked to explain the resistance of precalcined catalysts to acid dealumination.

INTRODUCTION

The zeolitic catalyst, H-ZSM-5, is the basis of a process (the Mobil Process) for the conversion of methanol to hydrocarbons in the gasoline boiling point range (*1–3*). Catalyst H-ZSM-5 has a high SiO_2/Al_2O_3 mole ratio and its activity has been attributed primarily to surface Brønsted sites (*4, 5*). Recent preliminary evidence (*6*) also suggests a role for Lewis sites in the initial step, methanol to dimethyl ether.

There have been several reports (*7–12*) dealing with the nature of Brønsted sites on H-ZSM-5. The ν(OH) region of the infrared spectrum has been the basis of a study by Vedrine *et al.* (*7*). Specifically, the positions and adsorption sensitivities of bands at 3720 and 3605 cm^{-1} lead to assignments to Brønsted sites with the site associated with 3605 cm^{-1} being the more acidic (*7*). The band at ca. 3600 cm^{-1}, unlike the absorption at ca. 3720 cm^{-1}, has been shown by Topsøe *et al.* (*10*) to decrease in intensity with catalyst dealumination. Recently Jacobs and Ballmoos (*11*) have reported evidence that the 3720-cm^{-1} band arises from extra-zeolitic material. However, a similar band has been observed for acid-extracted mordenites and in that closely related case has been attributed to surface groups created by dealumination (*13, 14*). It appears probable that these differences in interpretation might be resolved by a better understanding of the changes in surface structure associated with calcination, acid extraction, and dealumination of ZSM-5. This constitutes one objective in the present study.

METHODS

(*1*) *Material*

Na-ZSM-5 was prepared following the procedure of Argauer and Landolt (*15*) with a modification previously described (*6*).

[a] On study leave from the Department of Chemistry, University of Calgary, Canada.

0021-9517/84 $3.00

TABLE 1

The Results of XRF Analysis

Catalyst	Origin/treatment	Weight percent			Mole ratio
		SiO_2	Al_2O_3	Na_2O	SiO_2/Al_2O_3
Na-ZSM-5	Argauer (*15*)	86.19	8.95	4.86	16.34
H-ZSM$_1$-5	(i) Calcined at 1173 K/air (ii) 0.5 *M* HCl/353 K	90.44	9.33	0.23	16.45
H-ZSM$_2$-5	(i) Calcined at 773 K/O_2 (ii) 0.125 *M* HCl/293 K	88.95	8.02	3.03	18.82
H-ZSM$_3$-5	(i) Calcined at 773 K/air (ii) 0.25 *M* HCl/293 K	91.48	6.85	1.67	22.66
H-ZSM$_4$-5	0.25 *M* HCl/293 K	95.15	4.16	0.69	38.81
H-ZSM$_5$-5	0.25 *M* HCl/313 K	95.24	3.92	0.84	41.22
H-ZSM$_6$-5	0.5 *M* HCl/353 K	96.82	2.54	0.64	64.69
Comm. H-M[a]	Zeolon 100 H	89.04	10.80	0.16	13.99
Dealum. H-M	11 *M* HCl/373 K	96.18	3.74	0.08	43.64

[a] Commercial H-mordenite.

The characterization of the crystalline solid using X-ray diffraction and related techniques has been described previously (*6*). Several H-ZSM-5 batches of different Si/Al ratio were synthesized from the parent Na-ZSM-5 by conventional ion exchange/dealumination methods (Table 1). Several factors (the calcination temperature prior to ion exchange, and both the acid concentration and temperature) were found to influence the final catalyst composition, as revealed by X-ray fluorescence (XRF) analysis (Table 1). The results show that mild acid treatment before calcination can extract up to 70% of the aluminum from the original sample.

Commercial H-mordenite from Norton Company (Zeolon 100) was used without further purification.

Both the pyridine (Ajax AR grade) required for the study of surface acidity and the methanol (Merck high purity) used for the study of catalytic activity were distilled and dried over 4A molecular sieves, and were then outgassed with several freeze–pump–thaw cycles before being used.

(*2*) *Equipment*

The infrared spectra were obtained at 1 cm^{-1} resolution on a Nicolet MX-1E Fourier-transform–infrared spectrometer. The greaseless cell used for these studies is similar to the ir cell described previously (*16*). This cell was modified so that it holds up to four sample wafers at a time, so different samples can be subjected to identical treatment before their spectra are measured.

X-Ray fluorescence analyses were carried out by the Broken Hill Proprietary Company, Ltd., Newcastle, New South Wales, Australia.

(*3*) *Techniques*

(*a*) *The catalyst background.* Samples weighing 15 mg were formed at very low pressure into 13-mm-diameter self-supporting wafers. The wafers were heated under vacuum (ca. 0.133 mPa) for 2-h periods at progressively higher temperatures (maximum 1073 K). After each heating period, the samples were cooled to 293 K and infrared spectra were measured.

(*b*) *Pyridine adsorption/desorption studies.* Wafers prepared as above were subjected to the following treatment stages: (i) Activation—wafers were subjected to evacuation as described above, but the maxi-

mum temperature was 673 K. (ii) Cleaning—wafers were heated in a static atmosphere of O_2 (ca. 100 kPa) for 3 h to remove any carbonaceous contaminants. Some wafers were simultaneously presteamed by adding H_2O to the O_2; these were used in the study of the O–H stretching region (see below). (iii) Adsorption/desorption—Pyridine vapor was introduced to the samples at ambient temperature; the cell was then closed and heated at 373 K for a minimum of 2 h to allow pyridine to permeate the samples. The cell was then cooled, and a series of ir spectra were recorded after pumping for 2 h at each of the temperatures 293, 373, 473, 573, and 673 K. (iv) Water treatment—Some wafers were treated with H_2O vapor to convert Lewis pyridine to Brønsted pyridine and thus determine the extinction coefficient ratio for certain adsorbed pyridine bands (see below). After treatment as above, including desorption at $T \geq 573$ K, H_2O vapor was introduced and the cell was closed and heated at 373 K for 12 h. Physisorbed water was pumped off before the ir spectra were measured.

(*c*) *Measurement of catalytic activity by infrared spectroscopy.* The objective in this case was to determine the effect of dealumination on the ability of ZSM-5 to catalyze the conversion of methanol to hydrocarbons. This reaction proceeds in two steps: At lower temperatures, $373 < T < 560$ K, methanol is converted to dimethyl ether, and no hydrocarbon production can be detected (*6*). At higher temperatures, $T > 573$ K, the production of hydrocarbons from dimethyl ether will proceed (*6*).

The catalytic activity of each different zeolite sample was evaluated by measuring the intensity of characteristic infrared absorption bands in the vapor within the cell as the reactions proceeded. Bands were chosen which did not overlap with those of the other constituents present.

To monitor the first stage, i.e., the methanol to dimethyl ether step, a fixed quantity of methanol vapor was admitted to the cell. The intensity of the characteristic dimethyl ether band at 1102 cm^{-1} (*6*) was measured and compared to that of a band of unreacted methanol at 1033 cm^{-1} as a function of time, as the reaction proceeded at 523 K. After this stage had proceeded for several hours, the temperature was raised to 593 K to determine the activity of each sample for the dimethyl ether to hydrocarbon stage; the intensity of the hydrocarbon band at 2967 cm^{-1} was monitored relative to that of the strong dimethyl ether CH_3 rocking mode at 1178 cm^{-1} (*6*).

RESULTS AND DISCUSSION

Both calcined and noncalcined ZSM-5 batches degassed at 373 K reveal a broad infrared absorption at ca. 3550–3580 cm^{-1} which can be attributed to vibrations of hydrogen-bonded silanol or Brønsted groups (see Fig. 1). Consistent with this assignment, the band shifts to higher frequency and sharpens on degassing (associated with

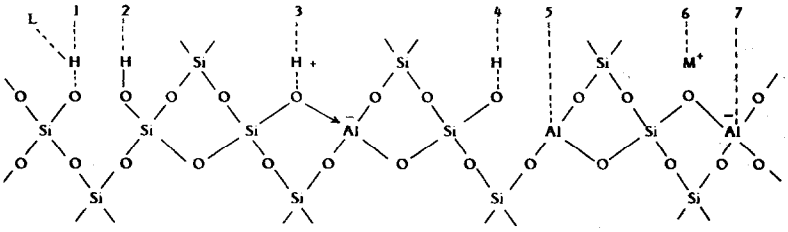

FIG. 1. Schematic catalyst structure, (1) Dealumination "nest" Brønsted site perturbed by adsorbate "L" (e.g., H_2O). (2) Dealumination "nest" silanol site. (3) Exchanged proton site. (4) Aluminum (Lewis)-associated Brønsted site. (5) Lewis site. (6) Cation (Na^+ or TPA^+) site. (7) Anionic aluminum site.

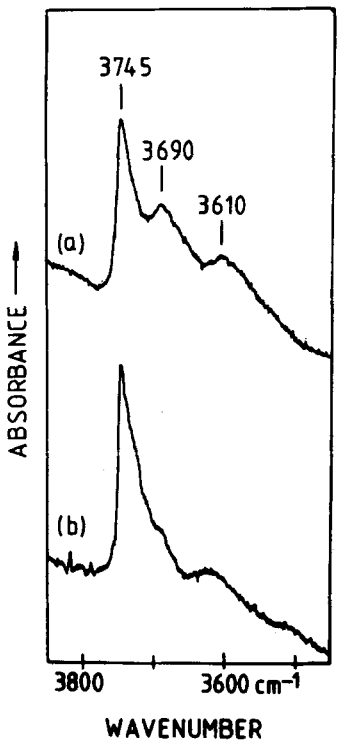

FIG. 2. Infrared spectra in ν(OH) region for H-ZSM$_6$-5 previously subjected to evacuation at (a) 673 K and (b) 873 K.

loss of surface H_2O) at 473–573 K. The spectrum of the catalyst after activation at 673 K exhibits surface silanol modes at 3730–3745, 3690, and 3610 cm^{-1}, as shown in Fig. 2 for H-ZSM$_6$-5. The assignment of these three bands can be confirmed by an analysis of their dependence on SiO_2/Al_2O_3 ratios as summarized in Fig. 3. The band at 3730–3745 cm^{-1} increases substantially in intensity with increasingly severe dealumination. This observation argues against its assignment to extra-zeolitic material as proposed by Jacobs and Ballmoos (*11*). The linear increase in intensity (Fig. 3) found for the band at 3730–3745 cm^{-1} with increasing SiO_2/Al_2O_3 ratio (i.e., aluminum loss) indicates an assignment to an acidic group created by the dealumination reaction. It is therefore assigned to the silanol "nest" (*13*) (referred to in Fig. 1 as sites 2) created by the removal of an aluminum atom on the internal or external zeolitic surface. The acidic nature of the sites associated with the band at 3730–3745 cm^{-1} is indicated by the observation that H-ZSM-5 batches pretreated at 1073 K and showing only the 3735-cm^{-1} mode adsorb pyridine in a protonated form identified by its characteristic spectrum. This is in accord with the earlier findings of Vedrine *et al.* (*7*). The bands at 3730–3745 and 3690 cm^{-1} overlap for samples activated at higher temperatures (723 K) and appear as a merged profile (3730–3745 cm^{-1}). This profile broadens with catalyst dealumination.

The 3610-cm^{-1} band also changes in intensity in an informative way with dealumination (Fig. 3). The observation that it decreases in intensity with progressive dealumination for samples H-ZSM$_i$-5, i = 4, 5, and 6 is consistent with its assignment to an aluminum-associated Brønsted silanol as proposed by Vedrine *et al.* (*7*) and Topsøe *et al.* (*10*). This is represented as sites 4 in Fig. 1. The initial intensity in-

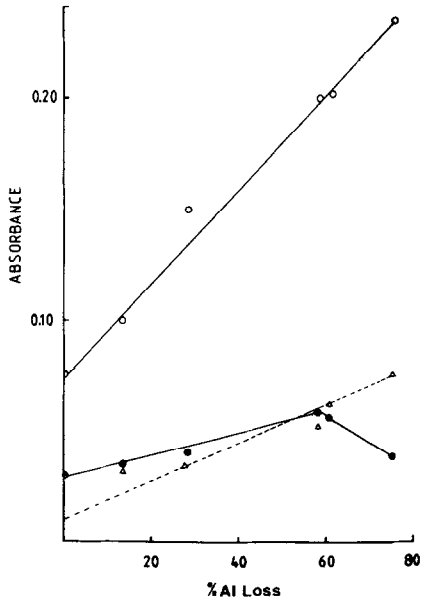

FIG. 3. Variation of silanol ν(OH) absorbance with dealumination of H-ZSM$_i$-5 catalysts: upper solid line 3730–3745 cm^{-} (site 2); dotted line 3690 cm^{-1} (site 1); lower solid line 3610 cm^{-1} (site 4).

crease may be associated with the persistence in H-ZSM$_i$-5 (i = 2 and 3) of substantial Na^+ content (Table 1). In this study, it is assumed that proton-exchanged sites 3 revert to sites 4 (acidic silanols) and sites 5 (Lewis sites) (*20*). Such an assumption is necessary for an interpretation of the reactivity sequence for the conversion of methanol to dimethyl ether (see later discussion). It would follow that residual Na^+ content in Na-ZSM-5 and H-ZSM$_i$-5 (i = 2, 3) would occupy sites 6 (Fig. 1) which cannot undergo a tautomeric shift to sites 4, 5. Also the high temperature of calcination for H-ZSM$_1$-5 may lead to a dehydroxylation of sites 4. The combination of these factors explains the initial rise in the 3610-cm^{-1} absorbance shown in Fig. 2. Once ion exchange is complete (H-ZSM$_i$-5, i = 4, 5, and 6) the trend of decreasing absorbance at 3610 cm^{-1} (Fig. 3) would reflect decreasing populations of site 4 silanols and Lewis sites.

The lower frequency (3610 cm^{-1}) of the site 4 silanol, its disappearance on pyridine adsorption and its recovery at late stages of pyridine desorption are all consistent with the site 4 being highly acidic. In comparison, the band at 3730–3745 cm^{-1} was also observed to diminish on pyridine adsorption but reappeared at earlier stages of pyridine desorption. Therefore, as suggested previously by Vedrine *et al.* (*7*) the Brønsted sites associated with the band at 3730–3745 cm^{-1} are less acidic than those associated with the 3610-cm^{-1} band.

The assignment of the previously unreported absorption at 3690 cm^{-1} also emerges from the trends evident in Fig. 3. If the activation temperature is relatively low ($T \leq 673$ K) or if the sample is presteamed in O_2/H_2O (see Methods, 3(b)(ii)) this band appears quite clearly (see Fig. 2). At higher activation temperature this band becomes weaker and is substantially overlapped by the band at 3730–3745 cm^{-1}, until after evacuation at 873 K it virtually disappears (Fig. 2). The behavior of the 3690-cm^{-1} band under these conditions suggests that it is a component of the profile at 3730–3745 cm^{-1} which is selectively perturbed by the interaction of the silanol "nest" with water. This suggestion is supported by infrared data to be discussed in section 2b. The observation (Fig. 3) that this band intensifies with aluminum removal also supports its assignment to the dealumination "nest." Also, the ratio of the absorbance of the band at 3730–3745 cm^{-1} to that of the 3690-cm^{-1} band is ca. 3 (see Fig. 3). Assuming similar extinction coefficients for the two bands, this result suggests that the nest consists of four silanols, one of which is perturbed by interaction with water (site 1, 3690 cm^{-1}) with the other three continuing to vibrate at the unperturbed frequency of 3730–3745 cm^{-1} (site 2).

Essentially, the interpretation above indicates that three types of Brønsted sites exist on the surface: silicon-associated Brønsted sites 2, water-perturbed silicon-associated Brønsted sites 1, and aluminum (Lewis)-associated Brønsted sites 4 (see Fig. 1). It also suggests that Lewis sites (site 5) exist on the surface.

As a result of this study of catalyst background features, the following sequences of site populations emerge: dealumination Brønsted sites 1, 2 (3690, 3730–3745 cm^{-1}) H-ZSM$_i$-5: i, 6 > 5 > 4 > 3 > 2 > 1. Lewis site 5 and Brønsted site 4 (3610 cm^{-1}) H-ZSM$_i$-5: i, 4 > 5 > 6.

(2) *Surface Site ([B]/[L]) Characterization by an Infrared Study of Pyridine Adsorption/Desorption and Water Treatment*

The pyridine vibrational mode assignments employed in this section of the study are based on those previously adopted (*17, 19, 20*). The key assignments are (i) 1545 cm^{-1} is assigned to Brønsted sites (B), (ii) 1455 cm^{-1} to Lewis sites (L), (iii) and 1490 cm^{-1} to a combination of B and L components. The Lewis-pyridine mode at 1455 cm^{-1} which can appear as a doublet (*14*) (see Fig. 4a) is not employed in evaluation of sequences in populations of Lewis sites

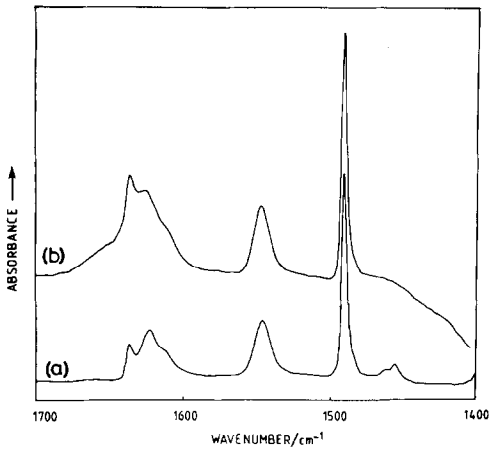

FIG. 4. Infrared spectra of pyridine on H-ZSM$_5$-5 (background subtracted). (a) After pyridine desorption at 573 K; (b) after H_2O treatment described under Methods 3b (iv).

because it is quite weak and because of its overlap with the 1440-cm^{-1} band arising from hydrogen-bonded pyridine after sample evacuation at low temperatures.

Lefrancois and Malbois (*21*) used H_2O treatment to convert Lewis pyridine into Brønsted pyridine and were then able to measure the [B]/[L] ratio for mordenites by comparing the intensities of the 1545-cm^{-1} Brønsted-pyridine band before and after H_2O treatment.

If A and A' refer to H-ZSM-5 sample absorbances before and after such H_2O treatment, respectively, then the number of B sites will be proportional to the absorbance of the 1545-cm^{-1} band before H_2O addition (A_{1545}), while the number of Lewis sites will be proportional to the gain in B sites resulting from the H_2O treatment, i.e., to ($A'_{1545} - A_{1545}$), assuming conversion of Lewis to Brønsted sites is complete, i.e.,

$$\frac{[B]}{[L]} = \frac{A_{1545}}{(A'_{1545} - A_{1545})} \qquad (1)$$

We have attempted to use this method with the present series of ZSM-5 samples. Unfortunately, even after prolonged water treatment, the ir spectra still showed the presence of pyridine bonded to Lewis sites; the bulky pyridine molecules evidently block the channels and retard H_2O diffusion. Only if some of the pyridine is desorbed at $T \geq 573$ K does the subsequent steaming process convert all Lewis sites to Brønsted sites, as can be seen in Fig. 4, where the Lewis-pyridine absorption at 1455 cm^{-1} disappears completely after the water treatment.

Such high temperature pyridine desorption is undesirable, however, because it could effect the apparent Brønsted-to-Lewis ratio, particularly if, as postulated here, two different types of Brønsted site exist on the surface. To resolve this difficulty, an alternative method was developed, which has the advantage that the [B]/[L] ratios can be calculated as a function of temperature.

From the hydrolysis experiment described above it can be seen that the extinction coefficient ratio

$$\left[\frac{\varepsilon^{B1490}}{\varepsilon_{1545}}\right] = \left[\frac{A'_{1490}}{A'_{1545}}\right] \qquad (2)$$

where ε^{B1490} refers to the Brønsted component of the 1490-cm^{-1} band. Although the numerical value of this ratio is determined in an experiment in which all Lewis sites are converted to Brønsted sites by H_2O treatment, once it is determined it should be constant and may therefore be used in calculations in subsequent experiments regardless of the extent of Lewis-to-Brønsted conversion. Therefore, the absorbances of the B and L components of the 1490-cm^{-1} band can be separated

$$A^{B1490} = \left[\frac{\varepsilon^{B1490}}{\varepsilon_{1545}}\right] A_{1545} \qquad (3)$$

and

$$A^{L1490} = (A_{1490} - A^{B1490}). \qquad (4)$$

Therefore

$$\frac{A^{B1490}}{A^{L1490}} = \frac{(\varepsilon^{B1490}/\varepsilon_{1545})A_{1545}}{A_{1490} - (\varepsilon^{B1490}/\varepsilon_{1545})A_{1545}}. \qquad (5)$$

Given Beer's Law ($A = \varepsilon Cl$) and the constancy of path length l for two sites on a common wafer

$$C \propto \frac{A}{\varepsilon}$$

or

$$\frac{C_B}{C_L} = \frac{[B]}{[L]} = \left[\frac{A^{B1490}}{A^{L1490}}\left(\frac{\varepsilon^{L1490}}{\varepsilon^{B1490}}\right)\right]. \quad (6)$$

Therefore if the ratio of the extinction coefficients ($\varepsilon^{L1490}/\varepsilon^{B1490}$) is known it is possible to determine [B]/[L] from the spectra after desorption at any temperature.

The ratio $\varepsilon^{B1490}/\varepsilon_{1545}$ can be determined as shown in Eq. (2) above. The ratio of the extinction coefficient of the Lewis component of 1490 cm^{-1} to the extinction coefficient of 1545 cm^{-1} may also be calculated

$$\frac{\varepsilon^{L1490}}{\varepsilon_{1545}} = \left[\frac{A_{1490} - (\varepsilon^{B1490}/\varepsilon_{1545})A_{1545}}{A'_{1545} - A_{1545}}\right]. \quad (7)$$

Thus, dividing Eq. (2) by Eq. (7)

$$\frac{\varepsilon^{B1490}}{\varepsilon^{L1490}} = \left[\left(\frac{A'_{1490}}{A'_{1545}}\right)\left(\frac{A'_{1545} - A_{1545}}{A_{1490} - (\varepsilon^{B1490}/\varepsilon_{1545})A_{1545}}\right)\right] \quad (8)$$

Since samples H-ZSM$_i$-5, i = 2 and 3 are least affected by the possible pyridine desorption prior to H_2O pump-off discussed above, the average value for these two samples, $\varepsilon^{B1490}/\varepsilon^{L1490}$ = 2.74, has been used in subsequent calculations. This figure differs from previous estimates of the extinction coefficient ratio reported for other zeolites. However, these literature values (*18, 21–23*) show considerable variation, especially when the ratio of Lefrancois and Malbois (*21*) is corrected for concentration. In the present study, this ratio functions essentially as a scaling factor, which leaves catalyst sequences unchanged.

The [B]/[L] ratios for the various catalysts, H-ZSM$_i$-5, have been calculated from Eq. (6) for samples presaturated with pyridine and then subjected to desorption over a series of increasing temperatures. The variation of [B]/[L] with changing desorption temperature is given in Fig. 5.

It would be predicted for a conventional oxide surface that the [B]/[L] ratio would decrease with increasing temperature because Brønsted sites are usually less thermally stable than Lewis sites (*20*). This predicted pattern is observed in the present study for commercial H-mordenite (Fig. 5). Two curves (broken lines) are shown for commercial H-mordenite in Fig. 5, corresponding to two different values of ($\varepsilon^{B1490}/\varepsilon^{L1490}$). For the upper curve this ratio is assumed to be 2.74 as for the H-ZSM$_i$-5 samples; for the lower curve the ratio is 4.25, the value of Lefrancois and Malbois (*21*), corrected for concentration. As can be seen, varying this ratio affects the magnitude of the [B]/[L] ratio but not the trend. The H-ZSM-5 samples in the present study exhibit [B]/[L] maxima at 473 K, which increase in magnitude with increasing dealumination. It is clear from these results

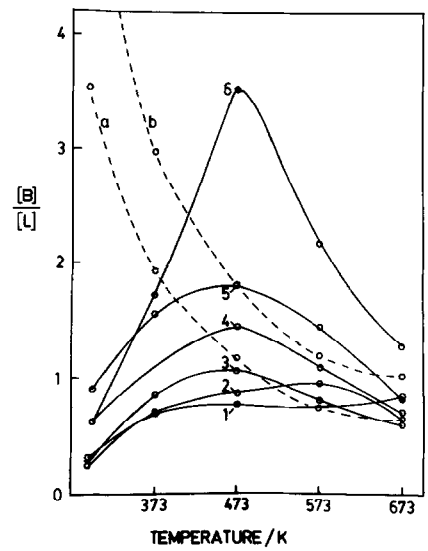

FIG. 5. Variation of [B]/[L] with pyridine desorption temperature for commercial H-mordenite (broken lines) and the series of H-ZSM$_i$-5 catalysts; catalyst numbers (i) identified on solid line. Curves for H-ZSM$_i$-5 catalysts, based on ($\varepsilon^{B1490}/\varepsilon_{1545}$) = 3.50 and ($\varepsilon^{B1490}/\varepsilon^{L1490}$) = 2.74 (see text). Curves for H-mordenite based on ($\varepsilon^{B1490}/\varepsilon_{1545}$) = 2.0 and $\varepsilon^{B1490}/\varepsilon^{L1490}$ = 4.25 (curve a) or 2.74 (curve b). See text for details.

that dealumination Brønsted sites of unusual thermal stability are created by acid extraction. These sites would coincide with the dealumination Brønsted sites 1 (Figs. 2 and 3) indicated by the catalyst absorption at 3690 cm^{-1} (see earlier).

The origin of the rise of each curve in Fig. 5 is necessarily a subject of some conjecture. However, it appears possible that pyridine competes with and at >373 K displaces H_2O associated with the Brønsted site 1:

$$(H_2O)_nH^+ \rightleftharpoons nH_2O + H^+ \xrightarrow{C_5H_5N:} [C_5H_5NH]^+$$

In this way the increased mobility of H_2O above 373 K may enhance its displacement by pyridine. The fall in [B]/[L] above 473 K in Fig. 5 would then reflect the greater stability of Lewis pyridine over Brønsted pyridine at elevated temperatures (*20*).

The sequence of dealumination Brønsted sites 1 and 2 suggested by the data in Fig. 5 is

$$\text{H-ZSM}_i\text{-5}, \qquad i\text{: } 6 > 5 > 4 > 3 > 2 > 1.$$

The temperature of the maxima in [B]/[L] ratios in Fig. 5 is ca. 473 K. This temperature is somewhat less than the optimum temperatures for the methanol conversion reaction. Being weaker electron donors than pyridine, the key species in the conversion pathway may require higher temperatures to displace H_2O from the $(H_2O)_nH^+$ in site 1 (above).

The conclusions drawn above may provide additional insight into the nonuniform sites of high-thermal stability invoked in a microcalorimetric study of dealuminated ZSM-5 (*24*). On the basis of the present evidence, these sites would appear to be dealumination Brønsted sites rather than Lewis sites as originally proposed (*24*).

(*3*) *Determination of Relative Site Populations from XRF Analysis Data*

In agreement with an earlier XPS investigation (*25*), and in contrast with an Auger spectroscopic investigation (*26*), Derouane *et al.* (*27*) have proposed that the aluminum distribution in ZSM-5, should not be considered in all cases to be homogeneous. This nonuniform distribution of aluminum depends on the method of catalyst preparation (*28*). Ballmoos *et al.* (*31*) in a crystallographic study have suggested that the aluminum content of the catalyst is concentrated on the peripheral surfaces of the ZSM-5 bulk crystal. Such an assertion is consistent with the highly selective acid extraction of aluminum from ZSM-5 observed in the present study. Exhaustive extraction leads to a solid phase which, in analytical terms, is almost pure silica (see Table 1). In the approach described here changes in elemental composition (from XRF) resulting from acid extraction of aluminum anions and proton exchange for Na^+ ions are assumed to be localized on the ZSM-5 surface. Specifically, loss of a surface aluminum leads to the formation of one "nest" of silanols and therefore a single Brønsted site 1 (see earlier discussion). Also exchanging one sodium ion with one proton (site 3) leads via a tautomeric shift to one Lewis site 5 and one associated Brønsted site 4.

For this stage of the project, ZSM-5 samples were subjected to a high-temperature (ca. 1273 K) analytical pretreatment which ensured that all TPA cations had decomposed into Brønsted sites 3 (which it is assumed, revert to sites 4 and 5) and therefore that the only cations present are Na^+. The decomposition of organic cations at $T \geq 673$ K was confirmed by infrared spectroscopy. The site population calculation, based on the elemental analysis in Table 1, can be described in terms of four stages.

(a) The mild acid treatment of the Na-ZSM-5 causes dealumination and ion exchange, and the catalyst calcination results in the decomposition and removal of the organic cations used in the zeolite synthesis. The changes in the percentage compositions in Table 1 reflect both of these factors. To focus on the catalytically

TABLE 2

The Relative Number of Atoms of Each Type

Catalyst	n(Si)	n(Al)	n(Na)	% Al loss[a]
Na-ZSM-5	100	12.25	10.95	—
H-ZSM$_1$-5	100	12.17	0.49	0.65
H-ZSM$_2$-5	100	10.65	6.61	13.10
H-ZSM$_3$-5	100	8.84	3.55	27.84
H-ZSM$_4$-5	100	5.14	1.40	58.04
H-ZSM$_5$-5	100	4.86	1.70	60.33
H-ZSM$_6$-5	100	3.10	1.30	74.69
Comm. H-M[b]	100	14.32	0.34	—
Dealum. H-M	100	4.60	0.16	67.88

[a] Relative to Na-ZSM-5 for the H-ZSM-5 samples, and to commercial H-mordenite for dealuminated H-mordenite. The commercial H-mordenite was used as received.

[b] Commercial H-mordenite.

important Al removal and Na^+ exchange, it is convenient to make the reasonable assumption that Si content remains constant (i.e., Si is not extracted). Then the Na and Al weight percentages (x) are normalized on the Si content of the original Na-ZSM-5; the normalized weights (X) in sample i are given by

$$X(\mathrm{Al})^i = \left[\frac{x(\mathrm{Si})^{\mathrm{Na}}}{x(\mathrm{Si})^i} \cdot x(\mathrm{Al})^i\right] \qquad (9)$$

and

$$X(\mathrm{Na})^i = \left[\frac{x(\mathrm{Si})^{\mathrm{Na}}}{x(\mathrm{Si})^i} \cdot x(\mathrm{Na})^i\right] \qquad (10)$$

where the superscript Na refers to the Na-ZSM-5 phase.

(b) The normalized weights from (9) and (10) can be converted into relative numbers of atoms of each type by dividing by the atomic weights

$$n(\mathrm{Al})^i = \frac{x(\mathrm{Al})^i}{26.98} \qquad (11)$$

$$n(\mathrm{Na})^i = \frac{x(\mathrm{Na})^i}{22.99} \qquad (12)$$

Since all weights have been normalized on the Si content of the original Na-ZSM-5, then in all cases

$$n(\mathrm{Si}) = \frac{40.29}{28.09} = 1.434.$$

However, it would be more convenient to have the numbers of Al and Na atoms compared to 100 Si atoms, and therefore each number calculated from Eqs. (11) and (12) is multiplied by 100/1.434 = 69.74 to effect this. The results of these calculations are collected in Table 2.

(c) Assuming that all Al is present as either Lewis sites 5 or anionic sites 7 and that any exchanged proton site 3 reverts to a Brønsted site 4 and a Lewis site 5 (Fig. 1), the number of Lewis sites (L) will be given by

$$n(\mathrm{Al})^i - n(\mathrm{Na})^i = [\mathrm{L}]. \qquad (13)$$

Following the finding of Hatada *et al.* (*8*), it is presumed that Brønsted sites 3 formed from the decomposition of TPA cations also revert to sites 4 and 5. Any equilibrium between site 3 and sites 4 and 5 would change the absolute values but not the sequence of L for various batches (i).

(d) The number of dealumination Brønsted sites 1 (see earlier infrared spectra of the catalysts) will be equal to the number of Al atoms extracted by the acid treatment

$$n(\mathrm{Al})^{\mathrm{Na}} - n(\mathrm{Al})^i = [\mathrm{B}]. \qquad (14)$$

From expressions (13) and (14) the parameters [L], [B], and [B]/[L] can be calculated. The sequences for the dealuminated catalysts are given in Table 3 and Fig. 6 which also includes the [B]/[L] results at 473 K from the pyridine ir Method (the 1490-cm^{-1} method, see earlier). These values have relative rather than absolute significance. The calculation of parameter [B] is based on Al extracted and so represents sites created by dealumination.

(*4*) *Comparison of Site Sequences with Conversion Reactivities*

In the preceding discussion three methods were employed to identify the changing pattern of surface site populations with progressive dealumination and ion exchange.

TABLE 3

Brønsted and Lewis Acid Sites Determined from XRF

Catalyst	[B] $n(Al)^{Na}$–$n(Al)^{i}$	[L] $n(Al)^{i}$–$n(Na)^{i}$	[B]/[L]
H-ZSM$_1$-5	0.08	11.68	0.01
H-ZSM$_2$-5	1.60	4.04	0.40
H-ZSM$_3$-5	3.41	5.29	0.64
H-ZSM$_4$-5	7.11	3.74	1.90
H-ZSM$_5$-5	7.39	3.16	2.34
H-ZSM$_6$-5	9.15	1.80	5.08
Comm. H-M[a]	0.00	13.98	0.00
Dealum. H-M[b]	9.72	4.44	2.19

[a] Commercial H-mordenite.
[b] Dealuminated H-M is prepared from commercial H-M.

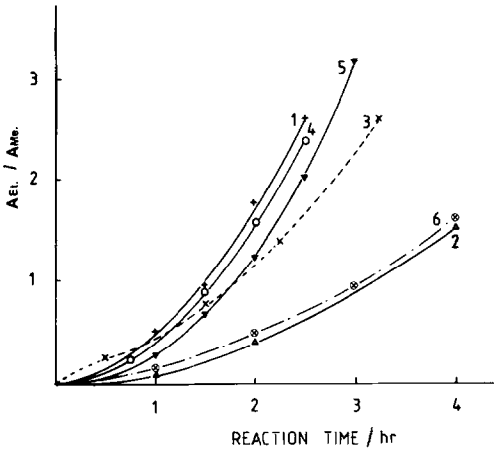

FIG. 7. Kinetic reactivities of various H-ZSM$_i$-5 catalysts for the conversion of methanol to dimethyl ether at 523 K. Catalyst numbers (i) appear beside each curve. A_{Et}/A_{Me} is the absorbance ratio of the dimethyl ether to methanol bands as described under Methods 3(c).

The objective at this stage will be first to identify the favored sequences of populations of various site types suggested by these methods, and second to relate those sequences to observed reactivities for the conversion process. The catalytic reactivity of each zeolite sample, H-ZSM$_i$-5, toward the two different steps of the reaction was measured by monitoring characteristic ir bands, as described under Methods (3c). The results are shown in Figs. 7 and 8. The sequences of sites and reactivities are summarized in Table 4.

The favored sequence of the Brønsted "nest" (sites 1 and 2) resulting from dealumination is indicated clearly by all three methods used.

Site 1: H-ZSM$_i$-5,

i: 6 > 5 > 4 > 3 > 2 > 1.

The favored sequence of Lewis sites 5 is indicated by the XRF surface analysis method and supported by limited data from the ν(OH) absorbance approach

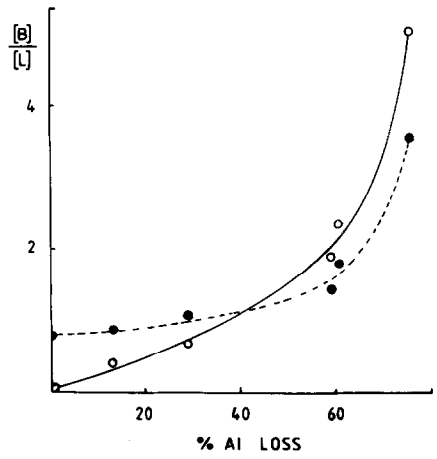

FIG. 6. Comparison of variations in [B]/[L] from FT–ir data (●) 1490 cm^{-1} method at 473 K and XRF data (○).

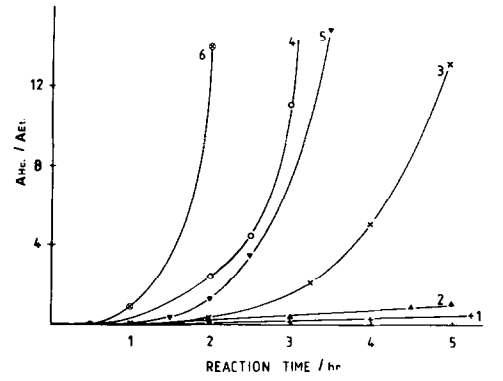

FIG. 8. Kinetic reactivities of various H-ZSM$_i$-5 catalysts for the conversion of dimethyl ether to hydrocarbons at 593 K. Catalyst numbers (i) appear beside each curve. A_{Hc}/A_{Et} is the absorbance ratio of the hydrocarbon to dimethyl ether bands as described under Methods 3(c).

TABLE 4

Sequences of Site Populations and Reactivities

Site method		Sequence of i in HZSM$_i$-5
(a) ν(OH), ir	*Sites 1,2:*	$6 > 5 > 4 > 3 > 2 > 1$
	Sites 4,5:	$4 > 5 > 6$
(b) Pyridine desorption, ir	*Site 1:*	$6 > 5 > 4 > 3 > 2 > 1$
(c) Surface analysis, XRF	*Sites 1,2:*	$6 > 5 > 4 > 3 > 2 > 1$
	Site 5:	$1 > 3 > 2 > 4 > 5 > 6$
Reactivities		
(a) $2CH_3OH \rightarrow (CH_3)_2O + H_2O$		$1 \geq 4 \geq 5 > 3 > 6 > 2$
(b) $(CH_3)_2O \rightarrow$ hydrocarbons		$6 > 4 \geq 5 > 3 > 2 > 1$

Site 5: H-ZSM$_i$-5,

$$i\text{: } 1 > 3 > 2 > 4 > 5 > 6.$$

The trend for the juxtaposed Brønsted site 4 would follow the same sequence. The reactivities toward the conversion process will now be examined in two stages.

(*a*) *The initial stage: CH_3OH to $(CH_3)_2O$.* Infrared spectroscopic analysis of the rate of this stage of the reaction (see Fig. 7) indicates a catalyst reactivity sequence

$$\text{H-ZSM}_i\text{-5}, \qquad 1 \geq 4 \geq 5 > 3 > 6 > 2.$$

This sequence differs from the Lewis site 5/ Brønsted site 4 sequence only in the positions of catalysts $i = 2$ and 3. These latter two batches are notable for their high Na^+ content. However, the presence of residual Na^+, as previously reported by the present authors (*6*) enhances the contribution of a carboxylate side reaction, and so diminishes the yield of $(CH_3)_2O$.

Consistent with this above sequence, dealuminated H-mordenite is a less effective catalyst for this first stage than commercial H-mordenite.

These results suggest that either sites 4 or sites 5 are responsible for this stage of the reaction. The conclusion that sites 5 rather than sites 4 are responsible is supported by the observation that the end-product of methanol decomposition is dimethyl ether for dehydroxylated H-ZSM-5 and for dehydroxylated γ-Al_2O_3 (*6*) which are presumed to have very low Brønsted activity. The involvement of Lewis sites in this initial stage has been the subject of an independent test which will be described in a future paper.

(*b*) *The latter stages: $(CH_3)_2O$ to hydrocarbons.* In a preliminary study (*6*), the present authors proposed that these latter stages were catalyzed by Brønsted sites. The sequence of reactivities for this stage has been shown by the present infrared spectroscopic study (see Fig. 8) to be

$$\text{H-ZSM}_i\text{-5}, \qquad i\text{: } 6 > 4 \geq 5 > 3 > 2 > 1.$$

This sequence clearly rules out a dominant involvement of Lewis sites 5 or Brønsted sites 4 (see Table 4). It clearly correlates with the sequence for the dealumination Brønsted site 1.

In this study, dealuminated mordenite was found to be a more effective catalyst for hydrocarbon formation than commercial mordenite as expected on the basis of [B] or [B]/[L] sequences as given in Table 3. However, comparisons between mordenites and H-ZSM-5 are complicated by the pronounced tendency of the former to form carbonaceous products and by the different channel structures and shape selectivities (molecular traffic control) of the two zeolite lattices (*29, 30*).

The limited reactivity of H-ZSM$_i$-5 batches which have not been significantly dealuminated (e.g., $i = 1$) probably arises from the aluminum-associated Brønsted site 4. The correlations above indicate that such a site is a less effective source of reactivity than the dealumination Brønsted sites 1.

CONCLUSION

(*1*) *The Reactivity of the Dealumination Brønsted Site (Site 1)*

The reason for the greater reactivity of dealumination Brønsted site 1 relative to the more acidic Lewis-associated Brønsted site 4 in the formation of hydrocarbons is necessarily a matter of some speculation. Possibly the localized negative charge on site 1, after site deprotonation by $(CH_3)_2O$

(*6*), is more effective in subsequent proton abstraction from methyl groups of $[CH_3O(H)CH_3]^+$ (*6*) than the delocalized negative charge on deprotonated sites 4, 5.

(*2*) *Calcining, Aluminum Migration, and Dealumination*

Electron microprobe scans across sections of ZSM-5 revealed that aluminum is concentrated in the rim portion of the crystals (*31*). In the present study, extreme acid dealumination of Na-ZSM-5 yields a catalyst which, in analytical terms, is almost pure silica (i.e., 96.82% for H-ZSM_6-5). Indeed in the case of H-ZSM_6-5, 72% of the aluminum in the original Na-ZSM-5 has been extracted. This percentage represents that part of the original aluminum in Na-ZSM-5 which was accessible to the acid reactant, or in other words, the percentage of the aluminum resident on the surfaces of Na-ZSM-5. Calcination of Na-ZSM-5 prior to acid extraction, yields a structure which is much more resistant to dealumination than uncalcined Na-ZSM-5. This resistance to dealumination is a common feature of other related uncalcined zeolites (e.g., mordenite). However, the aluminum-rich surface layers of ZSM-5 are not found in other zeolites (*31*) where aluminum is more or less uniformly dispersed throughout the structure. It therefore appears probable that calcining Na-ZSM-5, prior to acid extraction, may lead to a migration of aluminum atoms away from the surface layer and into crystal regions inaccessible to the acid reactant. Such aluminum migration is consistent with the lability of surface oxygen atoms (*32*) and the evidence for aluminum migration in other zeolites (*33*).

ACKNOWLEDGMENTS

One of the authors (R. A. K.) is grateful to NSERC (Canada) for the award of an International Collaborative Research Grant. The authors are also grateful to Ashim Ghosh for providing samples of dealuminated mordenite.

REFERENCES

1. Gibson, J., *Chem. Br.* **16,** 26 (1980).
2. Meisel, S. L., McCollough, J. P., Lechthaler, C. H., and Weisz, P. B., *Chem. Technol.* **6,** 86 (1976).
3. Chang, C. D., and Silvestri, A. J., *J. Catal.* **47,** 249 (1977).
4. Derouane, E. G., B.Nagy, J., Dejaifve, P., van Hooff, J. H. C., Spekman, B. P., Vedrine, J. C., and Naccache, C., *J. Catal.* **53,** 40 (1978).
5. Anderson, J. R., Mole, T., and Christov, V., *J. Catal.* **61,** 477 (1980).
6. Sayed, M. B., and Cooney, R. P., *Aust. J. Chem.* **35,** 2483 (1982).
7. Vedrine, J. C., Auroux, A., Bolis, V., Dejaifve, P., Naccache, C., Wierzchowski, P., Derouane, E. G., B.Nagy, J., Gilson, J. B., van Hooff, J. H. C., Berg, J. B., and Wolthuizen, J., *J. Catal.* **59,** 248 (1979).
8. Hatada, K., Ono, Y., and Ushiki, Y., *Z. Phys. Chem. (Wiesbaden)* **117,** 37 (1979).
9. Auroux, A., Bolis, V., Wierzchowski, P., Gravelle, P. C., and Vedrine, J. C., *J. Chem. Soc. Faraday Trans. I* **75,** 2544 (1980).
10. Topsøe, N., Pedersen, K., and Derouane, E. G., *J. Catal.* **70,** 41 (1981).
11. Jacobs, P., and Ballmoos, R. V., *J. Phys. Chem.* **86,** 3050 (1982).
12. Vedrine, J. C., Auroux, A., Dejaifve, P., Ducareme, V., Hoser, H., and Zhou, S., *J. Catal.* **73,** 147 (1982).
13. Chen, N.Y., *J. Phys. Chem.* **80,** 76 (1976).
14. Ghosh, A. K., and Curthoys, G., *J. Chem. Soc. Faraday Trans. I* **79,** 805 (1983).
15. Argauer, R. J., and Landolt, G. R., U.S. Patent 3,702,886 (1972).
16. Petfield, A. T., and Cooney, R. P., *Aust. J. Chem.* **33,** 653 (1980).
17. Parry, E. P., *J. Catal.* **2,** 371 (1963).
18. (a) Basila, M. R., Kantner, T. R., and Rhee, K. H., *J. Phys. Chem.* **68,** 3197 (1964), (b) Basila, M. R., and Kantner, T. R., *J. Phys. Chem.* **70,** 1681 (1966).
19. Basila, M. R., *J. Phys. Chem.* **66,** 2223 (1962).
20. Ward, J. W., *in* "Infrared Studies of Zeolites and Surface Reactions" (J. A. Rabo, Ed.), Chap. 3, ACS Monograph No. 171. Amer. Chem. Soc., Washington, D.C., 1976.
21. Lefrancois, M., and Malbois, G., *J. Catal.* **20,** 350 (1971).
22. Sayed, M. B., and Cooney, R. P., unpublished data.
23. Hughes, T. R., and White, H. M., *J. Phys. Chem.* **71,** 2192 (1967).
24. Auroux, A., Wierzchowski, P., and Gravelle, P. C., *Thermochim. Acta* **32,** 165 (1979).
25. Tempere, J. Fr., Delafosse, D., and Cotour, J.P., *Chem. Phys. Lett.* **33,** 95 (1975).

26. Suib, S.L., Stucky, G. D., and Blattner, R. J., *J. Catal.* **65,** 174 (1980).
27. Derouane, E. G., Gilson, J. P., Galbelica, Z., Desbuquoit, C. M., and Verbist, J., *J. Catal.* **71,** 447 (1981).
28. Hughes, A. E., Wilshier, K. G., Sexton, B. A., Smart, P. *J. Catal.* **80,** 221 (1983).
29. Derouane, E. G., and Gabelica, Z., *J. Catal.* **65,** 486 (1980).
30. Dejaifve, P., Auroux, A., Gravelle, P. C., Vedrine, J., Gabelica, Z., and Derouane, E. G., *J. Catal.* **70,** 123 (1981).
31. Ballmoos, R. V., and Meier, W. M., *Nature (London)* **289,** 782 (1981).
32. Ballmoos, R. V., and Meier, W. M., *J. Phys. Chem.* **86,** 2698 (1982).
33. Wichterlova, B., Novakova, J., Kubelkova, L., and Jiru, P., *in* "Proceedings, 5th International Conference on Zeolites" (L. V. Rees, Ed.), Heyden, London, 1980.